# Scaling of the Current Conduction Zone in Lithium-fed Arc Multichannel and Single-channel Hollow Cathodes

**IEPC-2007-135**

*Presented at the 30$^{th}$ International Electric Propulsion Conference, Florence, Italy*
*September 17-20, 2007*

Leonard D. Cassady*
*Ad Astra Rocket Company, Bay Area Plaza, 141 Bay Area Blvd., Webster, TX 77598, USA*

E. Y. Choueiri†
*Princeton University, Princeton, New Jersey 08544, USA*

**The scaling of the current conduction zone depth, axial length, and temperature with the controllable parameters of cathode wall thickness, channel diameter, current, and mass flow rate in lithium-fed arc multichannel and single-channel hollow cathodes was determined in order to elucidate the physical mechanisms operating inside such cathodes. Understanding current conduction in such cathodes is necessary for the development of theoretical models for use in magnetoplasmadynamic thruster design. The surface area through which current was conducted from the plasma to the cathode material was estimated from experimental data along with corresponding plasma density. The plasma density was also calculated based on gas flow through the channel to estimate the scaling of plasma penetration depth. It was found that the current is conducted only from an active zone, which has an axial extent of approximately three wall thicknesses. A relationship was derived that allows obtaining the plasma density from the cathode temperature. Using that relationship and the calculation of pressure within the channel based on gas flow, it was determined that the plasma penetrates to the location where the density matches that required by the current density.**

## Nomenclature

*Symbols*

| | |
|---|---|
| $\alpha$ | Transmission probability through a short duct |
| $\gamma$ | Ratio of specific heats |
| $\delta$ | Molecular diameter |
| $\eta_v$ | Fluid viscosity |
| $\theta$ | Weighting factor used in transitional flow calculations |
| $\lambda_a$ | Average mean free path |
| $\lambda_m$ | Mean free path |
| $\rho_a$ | Average gas density |
| $C$ | Conductance |
| $C_a$ | Aperture conductance for molecular flow |
| $C_m$ | Molecular conductance |
| $C_v$ | Viscous conductance |
| $C_{v,a}$ | Viscous conductance through aperture |
| $C_z$ | Conductance term in viscous flow |

*Lead Project Engineer, lcassady@adastrarocket.com
†Associate Professor, Mechanical and Aerospace Engineering Department and Director, Electric Propulsion and Plasma Dynamics Laboratory (EPPDyL), choueiri@princeton.edu

| | |
|---|---|
| $d_c$ | Inner diameter of the cathode channel |
| $f_D$ | Darcy friction factor |
| $j$ | Current density |
| Kn | Knudsen number |
| $k_B$ | Boltzmann constant |
| $k_s$ | Empirical constant in flow weighting factor |
| $m$ | Molecular mass |
| M | Mach number |
| $\mathrm{M}_x$ | Mach number at the upstream location $x$ |
| $n$ | Number density |
| $n_i$ | Ion number density |
| $n_{i,s}$ | Ion density at the sheath/presheath boundary |
| $p_i$ | Ion pressure |
| $p_d$ | Downstream pressure |
| $p_e$ | Pressure within the channel at the exit |
| $p_u$ | Upstream pressure |
| $\dot{Q}$ | Flow throughput |
| $\dot{Q}_m$ | Molecular gas flow throughput |
| $\dot{Q}_t$ | Total gas flow throughput |
| $\dot{Q}_v$ | Viscous gas flow throughput |
| Re | Reynolds number for pipe flow |
| $u$ | Thermal speed of gas molecules |
| $v_a$ | Average gas speed |
| $V_B$ | Voltage associated with Bohm velocity |
| $v_B$ | Bohm velocity |
| $v_{g,x}$ | Velocity of the gas at the channel exit |
| $x$ | Distance upstream of channel exit |
| $x_e$ | Effective distance upstream of exit for molecular flow |

# I. Introduction

High-power electric propulsion systems have long been recognized as among the most promising options for heavy-payload orbit raising and piloted planetary missions,[1–4] but research has been limited due to the lack of in-space power. Among these high-power thrusters is the lithium Lorentz force accelerator (LiLFA), a type of magnetoplasmadynamic thruster (MPDT) that utilizes lithium propellant and a multichannel hollow cathode (MCHC). An MCHC has many small axial channels through which propellant flows, providing a high density plasma that conducts current to the inner surfaces of the channels, as shown in 1b. The lithium propellant and MCHC have been experimentally shown to improve the performance and lifetime of the LiLFA over standard gas-fed MPDTs,[5] but the fundamental operation of such a cathode configuration was poorly understood. The motivation of this research is to develop an understanding of the fundamental physical processes of the lithium-fed arc MCHC so that an informed LiLFA cathode design is possible.

The MCHC has been studied as a plasma source[6–12] and in conjunction with thruster development,[5,10,13,14] but the fundamental physical processes within the cathode were not established; although Declroix et al.[6] experimentally demonstrated that the division of mass flow rate and current between channels in an MCHC reduced discharge voltage and cathode temperature compared to an SCHC. Since the SCHC is essentially one channel of an MCHC, it can also be studied to determine the nature of the arc within the channel. It is easier to diagnose and analyze results of an SCHC when compared to an MCHC because the effects of multiple channels do not complicate interpretation of the results. Of the few experiments that utilized a lithium-fed SCHC or MCHC,[5,8–10,15,16] most focused on thruster operation instead of the cathode. The temperature profile and plasma potential at the cathode tip of an arc hollow cathode had been measured at a few conditions,[8,9,17,18] but not enough data existed to allow the determination of trends in the dependence of the cathode voltage fall, temperature, and plasma penetration depth on the operating parameters. Recently, we[19,20] obtained extensive measurements that demonstrated new trends in lithium-fed arc MCHC and SCHC operation, however an explanation of the physical mechanisms that caused those trends was not provided.

In this paper we use the experimental data to determine the plasma conditions within the cathode, such as plasma penetration depth, how the current is conducted from the plasma to cathode material, and what processes determine the cathode temperature and voltage drop. First, we analyze the experimental data of Cassady[19] to find any normalization of that data that could provide insight into a fundamental physical process. Then we apply conservation of power to determine the plasma conditions (primarily ion density) within the channel from the measured voltage and temperature and develop a gas flow model for the channel to explain the plasma penetration depth.

We first present an overview of the SCHC and MCHC in section II. In section IIIA we show that the cathode temperature and voltage drop depend only on the current density on the internal surface of the cathode. In section IIIB we also determined the active zone width and the parameters that control it from the penetration depth and peak temperature data. We present an estimation of the plasma pressure and cathode surface work function based upon the cathode temperature in section IIIC. Using the pressure estimation, the conditions that determine plasma penetration depth are explained in section IIID. Finally, an analysis of the MCHC data is presented in section IV that uses the knowledge gained from the SCHC to explain the MCHC results.

# II. The Multichannel and Single-channel Hollow Cathode

Multichannel hollow cathodes conduct high currents at low voltage while having longer lifetime than other arc cathodes operating at similar conditions. They differ from planar or solid cathodes in that they have many channels that are open to the plasma in the inter-electrode space, as shown in Fig. 1. Most hollow cathodes operate with gas flow through the channels into the discharge volume. The plasma penetrates the cavities under many operating conditions, and that allows the arc to attach to the cathode in a confined volume. The geometry of the channels maintains a dense, highly ionized plasma near the cathode surface and thus more effectively allows a high current densities (10s to 100s A/cm$^2$) to be conducted from the plasma to the material.

Each channel in an MCHC is similar to a single-channel hollow cathode (SCHC), shown in Fig. 1a, which can been studied in more detail and is easier to diagnose experimentally. Physically, an SCHC is normally a thin-walled (0.01-1 mm) refractory metal (tantalum or tungsten) tube. The working gas flows through

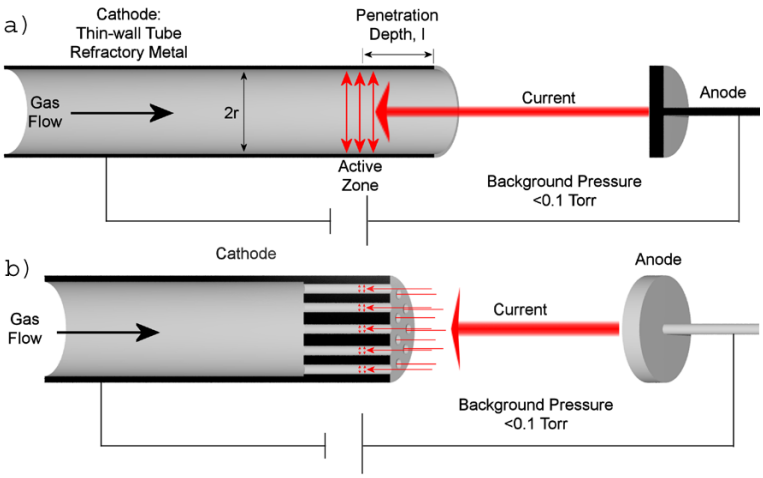


**Figure 1. a) A schematic of SCHC operation. b) A schematic of MCHC operation, including current penetration into the channels, gas flow through the channels, and low background pressure.**

the channel of the cathode, which creates a relatively high pressure within the channel (a few Torr) because the flow is choked as it exits into the inter-electrode space. The arc attaches to the interior surface of the channel at a distance from the tip, called the penetration depth, that depends upon mass flow rate, channel diameter, wall thickness, and current. Electrons are conducted from the cathode material via thermionic emission. The region where most of the current is drawn from the cathode surface is called the "active zone". The cathode voltage is the difference in potential between the material surface and the plasma potential at the cathode tip.

The controllable parameters of a hollow cathode arc discharge are the channel diameter and length, the cathode wall thickness and material, the gas mass flow rate and type, and the current. The discharge adjusts the voltage of the cathode relative to the plasma in the external discharge, the temperature profile of the cathode (including the penetration depth), the ionization fraction of the gas within the channel, and the electron temperature inside the channel, to provide the current demanded by the external circuit.

## III. Analysis of the SCHC Results

The range of flow rates and currents utilized in our SCHC experiments[19] provided a significant amount of data from which new insights can be derived. These insights are important because the conditions within the active zone were determined, which improves understanding of SCHC operation.

### A. Cathode Temperature and Voltage Drop Dependence on Current Density

The temperature and plasma potential data presented in the Appendix follow the same trends with current, and, therefore, we searched for an appropriate normalization that causes the data to collapse onto a single curve. Those data are included in the Appendix in Figs. 10 to 13. We found that by normalizing the current by dividing it by the inner circumference of the channel that the data collapse onto a curve. The bulk of the current is conducted from the cathode to the plasma in the active zone, which has a surface area that is determined by the circumference of the channel and its axial extent. Since the data collapse when normalized by circumference, the axial extent of the active zone in each cathode must be the same.

The 4 and 6 mm SCHC peak temperature and plasma potential at the cathode tip measurements at all flow rates collapse onto the same set of curves when plotted as a function of current density on the internal cathode surface, as shown in Figs. 2 and 3 including data at various mass flow rates between 0.2 and 1.6 mg/s. All of the current was assumed to be conducted from the plasma to the cathode wall in the active zone, the width of which was determined to be 1.5 mm based upon the cathode wall thickness, as described in section B. However, the temperature of the 6 mm cathode was slightly lower than that of the 4 mm SCHC. This can be attributed to the increased heat conducted axially along the larger cross-sectional area of the 6 mm cathode wall, which requires a larger relative ion flux to heat the wall while simultaneously

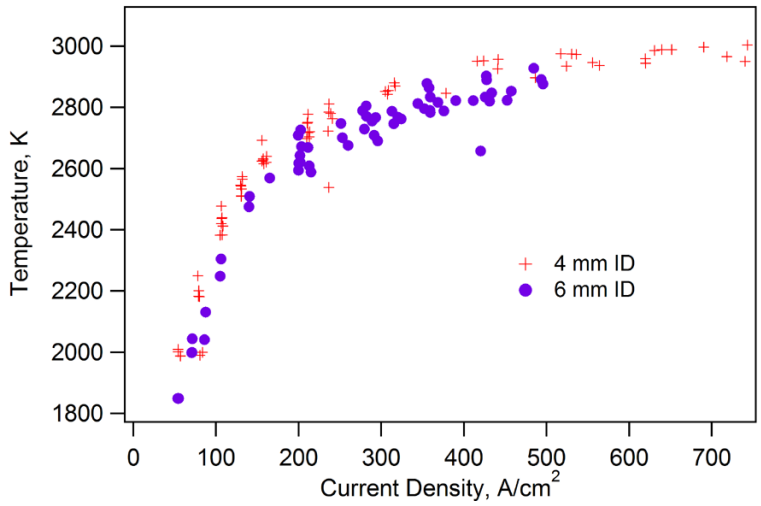


**Figure 2. Maximum temperature as a function of current density for the 4 and 6 mm SCHCs.**

reducing the thermionic electron current, and, thus, temperature. Nonetheless, the cathode temperature and plasma potential show a clear dependence on current density that is independent of penetration depth and mass flow rate.

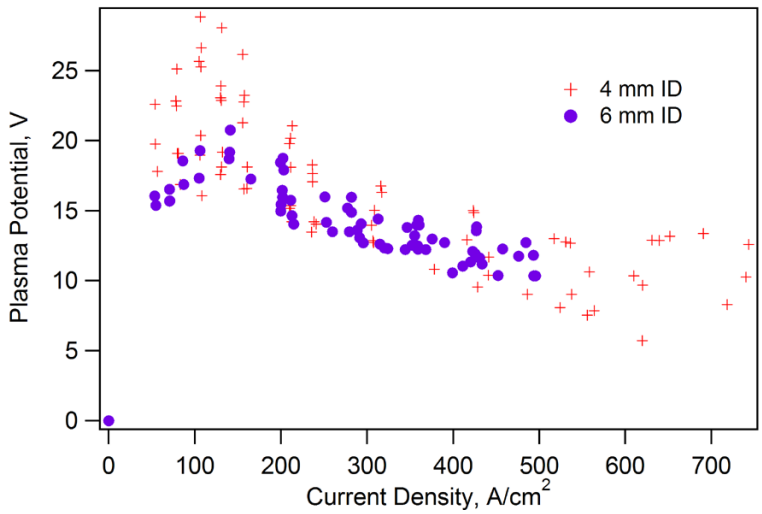


**Figure 3. The plasma potential at the cathode tip as a function of current density for the 4 and 6 mm SCHCs.**

## B. Active Zone Width

Here we present an analysis of the active zone width using the experimental results and a study of thermal conduction through a cathode wall. We show that an arc prefers to attach to the smallest area possible to reduce thermal radiative losses in order to find the lowest voltage (i.e. power loss) configuration. A smaller emitting surface gives a higher current density at a given current, but since the current density is exponentially dependent on temperature, the temperature will increase by a relatively small amount. At a fixed current and ion density the voltage must increase in order to provide the power for increased thermal radiation. Therefore, reducing the net thermal radiation decreases the voltage of the discharge. The effect of weakly increasing thermal radiation power density relative to the current density drive the active zone to a small width and the discharge to the lowest possible voltage.

There are two physical phenomena that could determine the minimum active zone width: the mean free

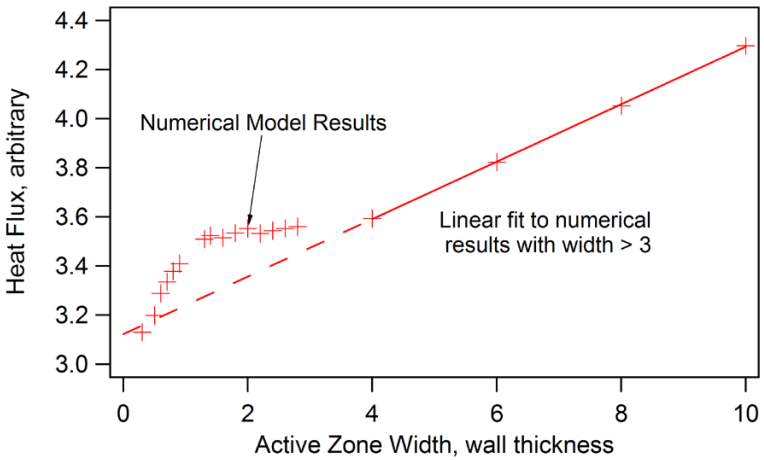


**Figure 4. Heat flux from a localized active zone.**

path of the high-energy electrons and thermal conduction through the cathode wall. It is not physically possible for the active zone width to be less than the mean free path of the high energy electrons because the plasma is generated by those electrons. As mentioned above, the discharge adjusts to minimize power loss, where thermal conduction from the active zone is the dominant loss mechanism (excluding thermionic cooling, which cannot be minimized because it depends only on the work function). The minimal thermal power loss configuration only conducts heat radially from the inner surface of the active zone to the outer surface where it is radiated away; any heat conducted axially is an added power loss. A numerical solution of 2-dimensional heat conduction in a high-aspect-ratio plane demonstrated that 1-dimensional effects dominate with active zone widths of greater than 3 to 4 wall thicknesses, because the power loss increases linearly with active zone width, as shown in Fig. 4. The thermal modeling program FEMlab was used to calculate the heat drawn from a 2900 K active zone surface of varying width centered on the long dimension of a plane 100 mm long and 0.5 mm wide. The outer surfaces radiated with an emissivity of 0.45 and the thermal conductivity was that of tungsten. Active zone widths from 1 to 3 wall thicknesses have approximately the same loss of heat, which is greater than would occur with purely 1-dimensional conduction - this is shown in Fig. 4 by the numerical results in that range of widths having a heat flux greater than that represented by the dashed line, which is an extension of the linear fit of the large width results. From this analysis we can state that if the active zone width is less than 3 wall thicknesses, heat conduction occurs 2-dimensionally and, therefore, increases the power lost. For a minimum power loss configuration, we use 3 wall thicknesses in our analysis.

### C. Ion Pressure in the Active Zone

Using the cathode temperature measurements and the calculated current density, we can determine the ion density within the active zone and the work function of the cathode. The ion pressure, $p_i$, is related to density through the equation of state,

$$p_i = n_i k_B T_c, \tag{1}$$

where $n_i$ is the ion density and the temperature is taken to be equal to the cathode temperature, $T_c$. The ions collide and thermalize with the wall many times as they travel down the channel,[7] therefore, setting the ion temperature to the cathode temperature is a good approximation. We include the most important processes at the cathode wall in the analysis, which are current conduction and power balance. The hot cathode surface emits electrons with a current density, $j_{th}$, as described by the Richardson-Dushman equation,[21]

$$j_{th} = A_R T_c^2 \exp\left(-\frac{e\phi_o}{k_B T_c}\right), \tag{2}$$

where $A_R$ is an empirical constant for the cathode material ($A_R = 70$ A·cm$^{-2}$K$^{-2}$ for tungsten), and $\phi_o$ is the material work function. The ion flux that impacts the wall after acceleration through the sheath

contributes to the total current density,

$$j = j_{th} + v_B e n_i \exp(-1/2), \tag{3}$$

where $v_B$ is the Bohm velocity, and $\exp(-1/2)$ accounts for the reduced density at the sheath edge due to presheath effects. The Bohm velocity is

$$v_B = \sqrt{\frac{k_B T_e}{m_{Li}}}, \tag{4}$$

which requires a presheath potential fall and density reduction to accelerate the ions. The potential drop through the presheath, $V_B = \frac{1}{2}\frac{k_B T_e}{e}$, is found from ion energy conservation. In turn, the ion density at the sheath/presheath boundary, $n_{i,s}$, is also reduced as described by the Boltzmann relation,

$$n_{i,s} = n_i \exp\left(-\frac{eV_B}{k_B T_e}\right) = n_i \exp(-1/2). \tag{5}$$

The power balance of an SCHC has three primary terms: the kinetic and potential energy delivered by the ions as they impact the wall, thermal radiation lost from the outer surface, and cooling via electron emission,

$$\epsilon_W \sigma_{SB} T_c^4 + j_{th}\left(\phi_o + \frac{3}{2}\frac{k_B T_c}{e}\right) = n_i v_B e\,(V_c - \phi_o + \phi_i)\exp(-1/2), \tag{6}$$

where $\epsilon_W$ is the emissivity of tungsten, $\sigma_{SB}$ is the Stefan-Boltzmann radiation constant, and $\phi_i$ is the ionization energy. (The absorbed plasma radiation, field-enhancement of thermionic emission, and conduction along the cathode are neglected in this analysis.) An example of the calculated ion pressure and surface temperature as a function of current density based on the solution of equations (1), (2), (3), and (6) is shown in Fig. 5. The plasma potential, which is identical to the cathode voltage drop, and electron temperature are assumed to be 10 V and 0.5 eV, respectively, which are representative values of the SCHC, but they actually vary with operating conditions. The results are insensitive to the electron temperature because the pressure and temperature are weakly dependent on that parameter. The predicted temperature dependence on current density has the same trends as the measured one, as shown in Fig. 6, which indicates that the most important processes have been included in the analysis.

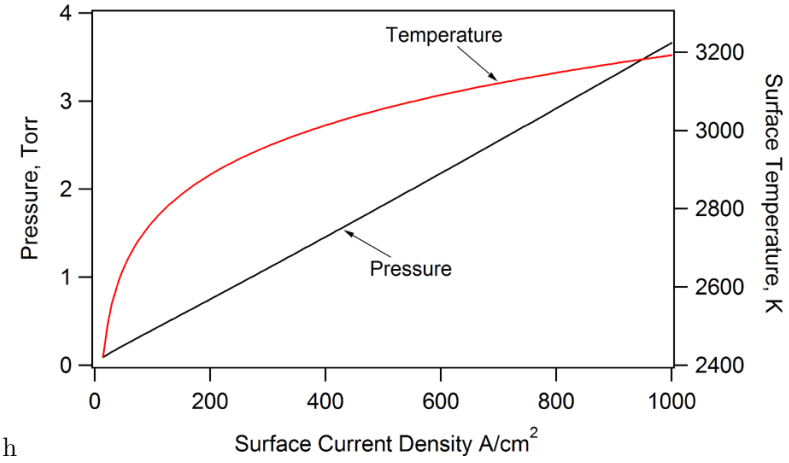


h

**Figure 5. Ion pressure and cathode temperature as a function of current density assuming 10 V cathode voltage drop and 0.5 eV electron temperature and 3.8 eV tungsten work function.**

The above equations give a unique relation between temperature, pressure, and current density, such that if one is known the others can be determined. Therefore, if the active zone temperatures of two different cathodes are the same, the ion pressure and current density are also the same. Consequently, the active zone occurs at a location of ion pressure that is sufficient to provide the heating required to balance the power losses of radiation and electron emission, which explains why the location depends on mass flow rate and channel diameter, but the temperature does not. The approximate power balance at the cathode wall

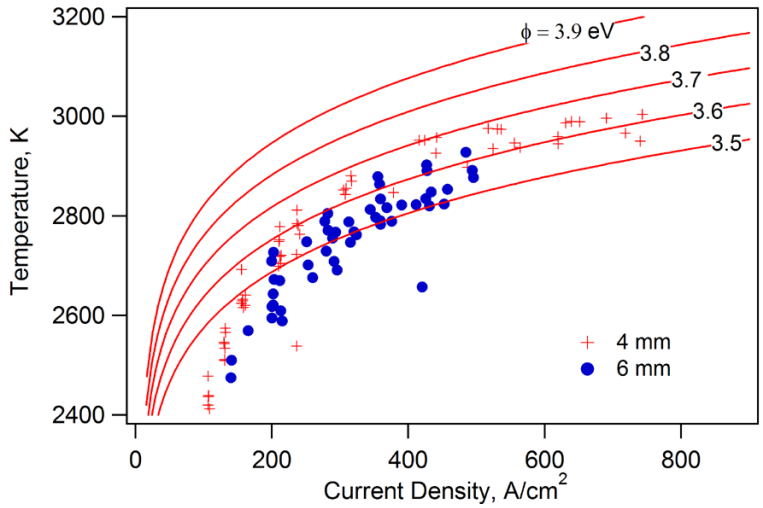


**Figure 6. Temperature prediction as a function of work function, $\phi$, and current density, assuming 1.5 mm active zone width compared to experimental data.**

demonstrates trends similar to the peak temperature versus current density data, as shown in Fig. 6. The temperature is less sensitive to current at high current because thermionic emission is dominating.

The measured cathode temperatures were lower than the values expected of a pure tungsten surface, likely because of a lower work function. The work function could have been reduced by oxygen impurities within the lithium or on the feed system walls, as the work of Babkin and Potapov[22] suggested. The work function of the material can be estimated using the experimental data and equations (2), (3), and (6) to determine the value of the work function that best fits the data. The comparison of the calculated surface temperature and the experimental data is shown in Fig. 6. A calculation of thermal conduction through the cathode wall determined that the internal surface temperature was approximately 80 K hotter than the measured external temperature. The temperature curve that is about 80 K greater than the mean of the data is the one associated with 3.7 eV. However, field enhancement of the thermionic emission reduced the work function by approximately 0.1 eV, as determined from calculations of the electric field within the sheath. Therefore, to account for the reduction due to field enhancement, a work function of 3.8 eV is a logical choice.

### D. Plasma Penetration Depth

The gas flow model determines the pressure along the channel so that the plasma penetration depth and density can be predicted. The density within the channel is determined by the gas mass flow rate, channel diameter, and cathode temperature. Since the gas exhausts into a region of much lower pressure, the flow is choked at the channel exit. Unfortunately, the conditions are such that the flow is not solely viscous or molecular, but is a "transitional" combination of both. There are no universally agreed upon or validated theories for choked, transitional flow through a short tube; This forces us to find the best approximation for our conditions.

The flow regime is determined by the Knudsen number,

$$\mathrm{Kn} = \frac{\lambda_m}{d_c}, \tag{7}$$

where $d_c$ is the diameter of the channel and $\lambda_m$ is the mean free path of the neutral atoms,[23]

$$\lambda_m = \frac{1}{\sqrt{2}\pi n \delta^2}, \tag{8}$$

with an atom number density and atomic diameter of $n$ and $\delta$, respectively. A Knudsen number of less than 0.01 indicates that the flow is viscous, while a value of greater than unity indicates that the flow is

molecular, otherwise the flow is considered to be transitional combination of both regimes. Hollow cathodes almost exclusively operate in the transitional regime, as corroborated by Ferreira and Delcroix.[24]

The gas flow in the channel of a hollow cathode is most accurately described as flow through a short duct. This is because the viscous losses do not dominate the kinetic effects. It is suggested by Lafferty[25] that any channel less than $20d_c$ long should be considered "short" and the appropriate model applied. Hollow cathodes generally have a length of less than $20d_c$. The experiments discussed in this dissertation have channel lengths of approximately $10d_c$. Lafferty[25] presented a general formulation for transitional flow through a short duct with a large pressure ratio,

$$\dot{Q}_t = \theta \dot{Q}_m + (1-\theta)\dot{Q}_v, \tag{9}$$

where $\dot{Q}_t$ is the total gas flow throughput, in units of pressure-volume per time, through the channel, which is weighted between molecular, $\dot{Q}_m$, and viscous, $\dot{Q}_v$, throughput. The total throughput is related to mass flow rate by

$$\dot{Q}_t = \frac{k_B T_c}{m}\dot{m}, \tag{10}$$

where $T_c$ is the cathode wall temperature, $m$ is the molecular mass of the gas, and $\dot{m}$ is the mass flow rate of the gas. The weighting factor is

$$\theta = \frac{k_s \mathrm{Kn}}{k_s \mathrm{Kn} + 1}, \tag{11}$$

where Santeler[26,27] chose $k_s = 28$, which corresponds to an equal proportion of viscous and molecular flow when the Knudsen number is in the mid-range of transitional flow.

Since we are determining the density along the channel, which is directly related to pressure, we must re-write equation (9) in terms of pressure. The flow throughput is related to pressure through the conductance,

$$C = \frac{\dot{Q}}{p_u - p_d}, \tag{12}$$

where $p_u$ and $p_d$ are the upstream and downstream pressures, respectively. The pressure downstream of the channel exit can be neglected because it is at least one order of magnitude smaller than the pressure within the channel. In the case of choked viscous flow, the throughput is independent of $p_d$. Equation (9) becomes

$$\dot{Q}_t = \left[\theta C_m + (1-\theta)C_v\right] p_u \tag{13}$$

when written in terms of the conductance of the viscous, $C_v$, and molecular, $C_m$, components of transitional flow. In order to find the upstream pressure the conductances as a function of channel length are required, and are described in the following subsections.

The flow is considered to be isothermal with a temperature equal to the cathode temperature. The model will poorly predict the pressure upstream of the plasma because of the large heat addition that is ignored. Ignoring heat addition is acceptable because we are not concerned with the gas upstream of the active zone.

### *1. Molecular Flow Conductance*

The molecular flow conductance is modeled as a short tube in series with an aperture at the exit. Here we use the molecular flow model presented by Lafferty.[25] The conductance is

$$C_m = \alpha C_a, \tag{14}$$

where $\alpha$ is called the transmission probability and $C_a$ is the aperture conductance. The aperture conductance is

$$C_a = \frac{\pi d_c^2}{4}\sqrt{\frac{k_B T_c}{2\pi m}}. \tag{15}$$

The conductance is lower farther upstream from the aperture because the molecules have less of a chance to directly exit the channel and are slowed by collisions with the wall. This is accounted for with the transmission probability term

$$\alpha = \frac{1}{1 + \frac{3}{4}\frac{x_c}{d_c}}, \tag{16}$$

where $x_e$ is the effective distance upstream of the channel exit defined by

$$x_e = x\left(1 + \frac{1}{3 + \frac{6}{7}\frac{x}{d_c}}\right) \tag{17}$$

and $x$ is the distance upstream of the exit aperture.

*2. Viscous Flow Conductance*

The viscous conductance is best described as compressible, frictional flow. We use the viscous flow model presented by Lafferty.[25] The thermodynamic relation between throughput, pressure, and Mach number, M, is

$$\dot{Q}_v = p_u\sqrt{\gamma}C_z\mathrm{M}\left[1 + \frac{1}{2}(\gamma-1)\mathrm{M}^2\right]^{1/2}, \tag{18}$$

where $\gamma$ is the ratio of specific heats of the gas and $C_z$ is a conductance term commonly found in viscous flow models,

$$C_z = \sqrt{2\pi}C_a. \tag{19}$$

Ideally, the throughput is referenced to the stagnation conditions, but we will use the active zone temperature because the stagnation conditions cannot be determined.

The Mach number at the upstream location, $\mathrm{M}_x$, is given by

$$\frac{1}{\gamma}\left\{\frac{1}{\mathrm{M}_x^2} - 1 - \frac{\gamma+1}{2}\ln\left[\frac{1}{\mathrm{M}_x^2}\frac{(\gamma-1)\mathrm{M}_x^2+2}{(\gamma+1)}\right]\right\} = \frac{f_D x}{d_c}, \tag{20}$$

where $f_D$ is the Darcy friction factor,

$$f_D = \frac{64}{\mathrm{Re}}, \tag{21}$$

for viscous laminar flow, where Re is the Reynolds number for pipe flow. The viscous component of transition flow is always laminar, because the maximum possible Reynolds number is approximately 160,[25] which is less than the value of 2000 at which turbulent flow occurs. The Reynolds number is given by

$$\mathrm{Re} = \frac{\rho_a v_a d_c}{\eta_v}, \tag{22}$$

where the fluid viscosity, $\eta_v$, depends on the gas type and temperature, and $\rho_a$ and $v_a$ are the average density and velocity, respectively. We will use the kinetic-theory relation for viscosity,[25,28]

$$\eta_v = 0.499\rho_a u\lambda_a = 0.998\sqrt{\frac{k_B T m}{\pi}}\frac{1}{\pi\delta^2}, \tag{23}$$

where $u$ is the gas molecule thermal speed and $\lambda_a$ is the average mean free path.

*3. Pressure and Velocity at the Channel Exit*

The exit pressure must be determined from the choked flow condition because the pressure outside of the channel, $p_d$, is much less than that required to choke the flow. A simple sonic condition is not accurate because the flow is transitional at the exit, therefore we use a relation similar to equation (9) to describe the flow, but the conductances are those of choked flow through an aperture,

$$\dot{Q}_t = \left[\theta C_a + (1-\theta)\,C_{v,a}\right]p_e. \tag{24}$$

The molecular flow component is simply described as the flow through an aperture [equation (15)]. The viscous flow conductance is

$$C_{v,a} = \left[\frac{\gamma(\gamma+1)}{2}\right]^{1/2} C_z. \tag{25}$$

It is not possible to analytically solve for $p_e$ in equation (24) because $\theta$ depends transcendentally on pressure through the Knudsen Number. First, we calculate the exit pressure assuming purely viscous flow

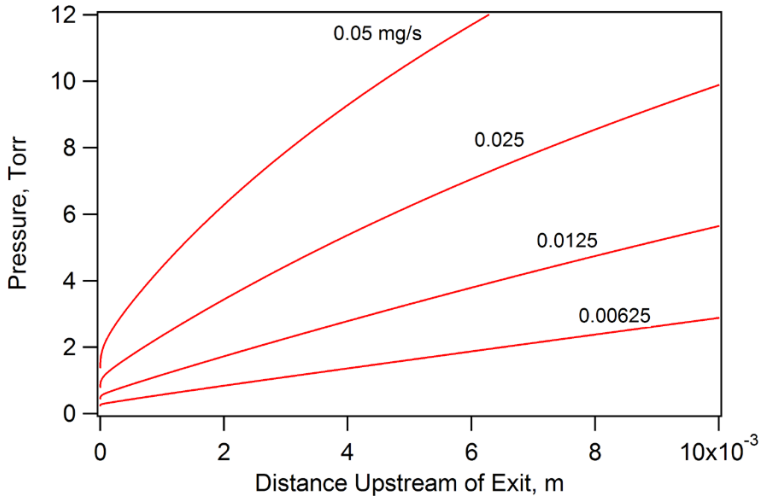


**Figure 7. Pressure profile of a 1 mm diameter channel**

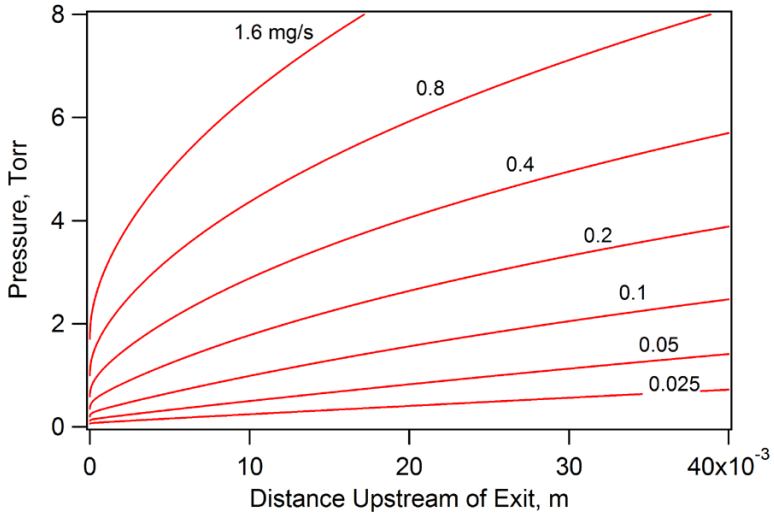


**Figure 8. Pressure profile of a 4 mm diameter channel**

in order to find an initial guess for the Knudsen Number and $\theta$. Then equations (24) and (11) are iteratively solved for $p_e$ until the pressure converges.

The velocity at the exit, $v_{g,x}$, is determined from the mass flow rate, temperature and pressure at the exit,

$$v_{g,x} = \frac{\dot{m} k_B T_c}{p_e m_{Li} \pi r_c^2}. \tag{26}$$

### *4. Pressure Profiles and Plasma Penetration*

A few characteristic pressure profiles (assuming a gas temperature of 3000 K) are presented in Figs. 7, 8, and 9 to illustrate their dependence on mass flow rate and channel diameter. The range of flow rates was chosen to represent values for which the cathode will operate optimally. This corresponds to pressures of a few Torr within the channel.[7] The pressure is taken to be only the partial pressure of the ions and neutrals within the theoretical model because the heavy particles dominate the flow calculations.

The plasma penetration depth can be explained using physical arguments. If the active zone were downstream of the optimal pressure, i.e. at a lower density, the cathode voltage drop would have to be

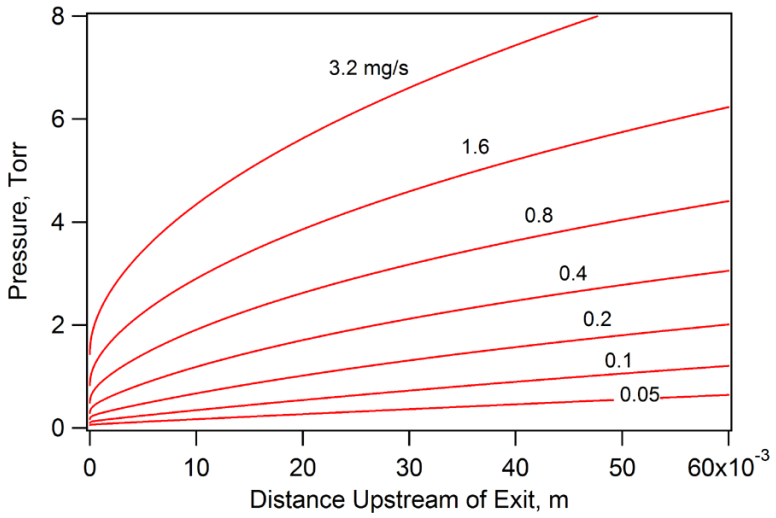


**Figure 9. Pressure profile of a 6 mm diameter channel**

greater in order for the ions to supply heat for thermionic emission and thermal radiation. Conversely, there would be no advantage of the active zone being upstream of the optimal density location because energy is lost to de-excitation radiation from a partially ionized plasma, and the axial electric field would increase the overall cathode voltage drop. The active zone moves upstream with increasing current to obtain the higher plasma density required to conduct more current. It can be seen that the pressure within the channel is approximately equal to that shown in Fig. 5, and that the dependence of penetration depth on mass flow rate is manifested in different pressure curves. Therefore, the active zone occurs at the location where the pressure matches that predicted in Fig. 5 for the given current and channel diameter.

## IV. Analysis of MCHC Results

A qualitative analysis of the MCHC results is presented because the cathode was not operated in optimal mode, which is defined by the lack of a significant plasma penetration. Our analysis of the pressure and current within the channels determined that the plasma could penetrate less than a millimeter at the highest current and lowest flow rate. (We did not operate at higher currents because of equipment limitations.) The differences between the high and low mass flow rate data can be attributed to how near the cathode operation was to optimal. Calculations of pressure within the channel, see Fig. 7, show that at the high mass flow rate (0.05 mg/s per channel) the pressure is greater than 2 Torr throughout the entire channel. Using Fig. 5, one can see that at that ion pressure the cathode could have supported at least 600 A/cm$^2$, compared to the maximum 175 A/cm$^2$ that we operated at. The current density is based upon an active zone width of 2 mm (Based on calculations presented by Cassady[19]). The data recorded at a 0.4 mg/s mass flow rate (0.021 mg/s per channel) could have had a penetration depth of a few tenths of a millimeter according to our model, but that is less than the accuracy of the measurements. The extension of the SCHC analysis to the MCHC correctly explains the plasma penetration depth data and how the MCHC can conduct such great currents.

## V. Conclusions

The analysis of the SCHC results revealed that

- the cathode temperature and voltage drop depend on current density at the active zone/cathode wall surface
- the active zone width is approximately three cathode wall thicknesses, independent of current or mass flow rate

- the plasma density can be determined from cathode temperature using Fig. 5
- the plasma penetrates to a location of optimal plasma density that depends on current and channel diameter
- in our experiments the surface work function was not equal to that of pure tungsten (4.5 eV), but was 3.8 eV.

The above insights applied to the MCHC data explain that the plasma did not measurably penetrate the channels because the mass flow rate was too great and current too small.

The motivation of this research was to gain understanding of the arc hollow cathode physics to design an MCHC. The analysis presented in this paper forms the basis of a detailed theoretical model capable of predicting cathode voltage fall and temperature. The theoretical model is presented by Cassady[19] and can be applied to the development of MCHCs for use in LiLFAs.

## Appendix

The maximum temperature of the four and six millimeter inner diameter cathodes is shown in Figs. 10 and 11. The mass flow rate and current ranged from 0.2 to 1.6 mg/s and from 10 to 150 A, respectively. The plasma potential at the cathode tip for the same cathodes operated throughout the same range is shown in Figs. 12 and 13.

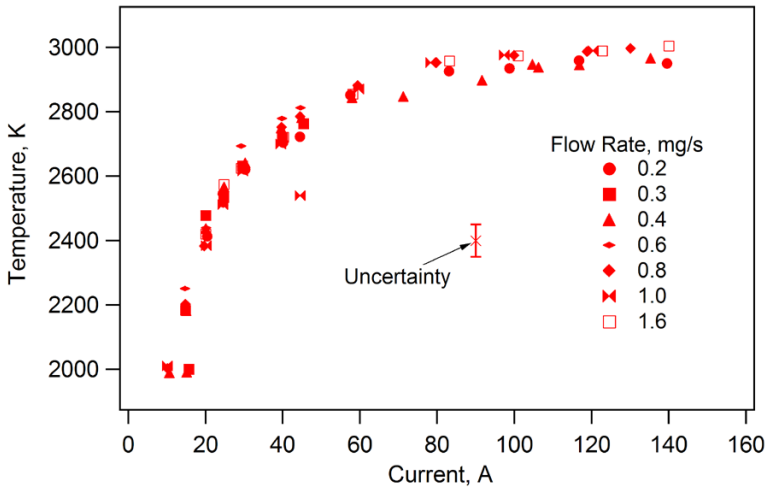


**Figure 10. The maximum temperature of the 4 mm SCHC.**

## References


[1]R. Frisbee. SP-100 nuclear electric propulsion for mars cargo missions. In *29th AIAA/SAE/ASME/ASEE Joint Propulsion Conference*, Monterey, CA, USA, June 1993. AIAA-93-2092.

[2]R. Frisbee. Electric propulsion options for mars cargo missions. In *32nd AIAA/ASME/SAE/ASEE Joint Propulsion Conference and Exhibit*, Lake Buena Vista, FL, USA, July 1996. AIAA-96-3173.

[3]J.E. Polk and T.J. Pivirotto. Alkali metal propellants for MPD thrusters. In *AIAA/NASA/OAI Conference on Advanced SEI Technologies*, Cleveland, OH, USA, September 1991. AIAA-91-3572.

[4]K. Sankaran, L.D. Cassady, A.D. Kodys, and E.Y. Choueiri. A survey of propulsion options for cargo and piloted missions to mars. In E. Belbruno, D. Folta, and P Gurfil, editors, *Astrodynamics Space Missions and Chaos*, volume 1017, pages 450–567, New York, NY, USA, 2004. Annals of the New York Academy of Sciences.

[5]V.P. Ageyev, V.G. Ostrovsky, and V.A. Petrosov. High-current stationary plasma accelerator of high power. In *23rd International Electric Propulsion Conference*, pages 1071–1075, Seattle, WA, USA, September 1993. AIAA/AIDAA/DGLR/JSASS. IEPC-93-117.

[6]J.L. Delcroix, H. Minoo, and A.R. Trindade. Gas fed multichannel hollow cathode arcs. *Review of Scientific Instruments*, 40(12):1555–1562, December 1969.

[7]J.L. Delcroix and A.R. Trindade. *Advances in Electronics and Electron Physics*, volume 35, chapter Hollow Cathode Arcs, pages 87–190. Acedemia Press, New York, NY, USA, 1974.

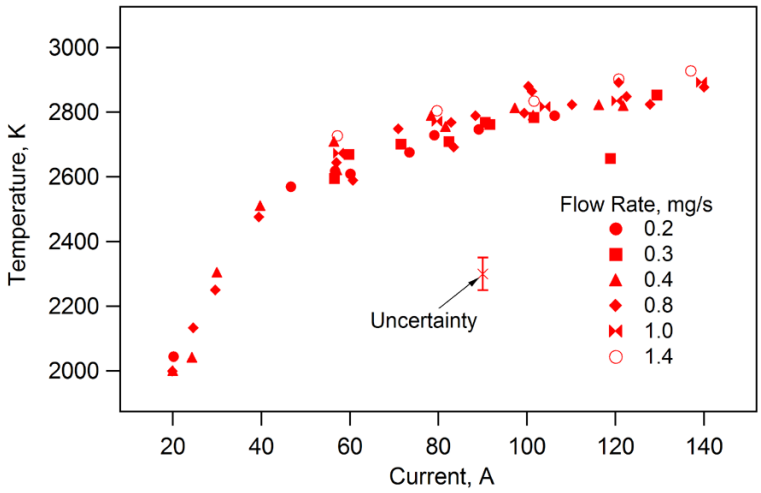


**Figure 11. The maximum temperature of the 6 mm SCHC.**

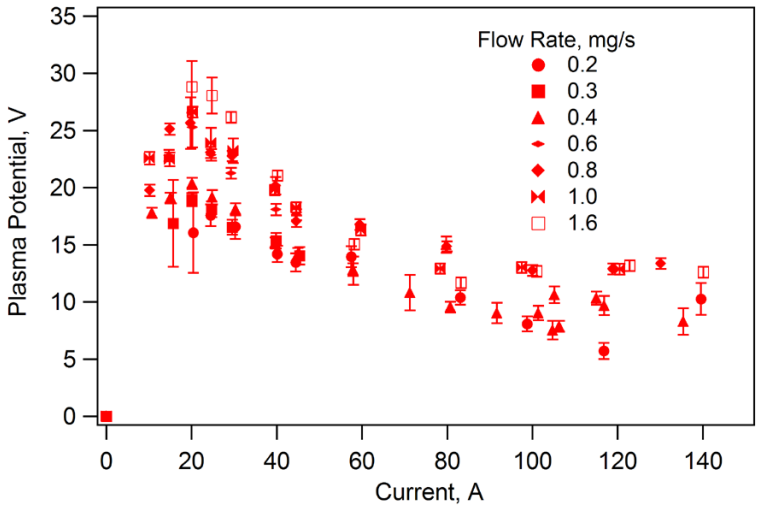


**Figure 12. The plasma potential at the cathode tip of the 4 mm SCHC.**

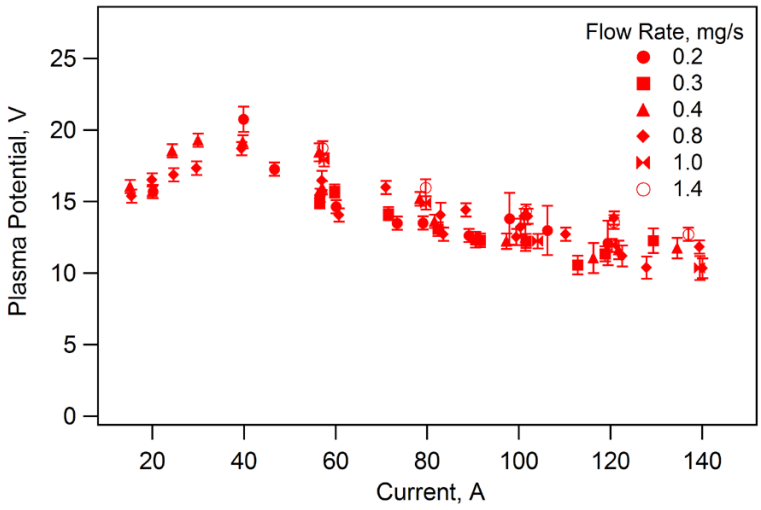


**Figure 13. The plasma potential at the cathode tip of the 6 mm SCHC.**

[8]G.V. Babkin, V.G. Mikhalev, S.N. Ogorodnikov, R.V. Orlov, and A.V. Potapov. High-current coaxial plasma source. *Soviet Physics - Technical Physics*, 20(9):1175–1178, 1976.

[9]G.V. Babkin, V.G. Mikhalev, E.P. Morozov, and A.V. Potapov. An experimental investigation of a plasma in a multi-channel cathode. *Journal of Applied Mechanics and Technical Physics*, 17(6):767–770, 1976.

[10]S.D. Grishin, A.K. Litvak, S.N. Ogorodnikov, and V.N. Stepanov. Intermediate-power steady-state plasma accelerator. *Soviet Physics - Technical Physics*, 22(2):280–285, February 1977.

[11]V.M. Ogarkov, S.N. Ogorodnikov, and V.N. Stepanov. The influence adsorption effects on the characteristics of a high-current multirod cathode. *Radio Engineering and Electronic Physics-USSR*, 23(8):123–127, 1979.

[12]V.M. Ogarkov, S.N. Ogorodnikov, and V.N. Stepanov. The design of the multirod cathode of a high-current plasma source. *Radio Engineering and Electronic Physics-USSR*, 21(12):98–103, 1976.

[13]S.A. Semenikhin and V.B. Tikhonov. The influence of cathode design on the performance and characteristics of MPD thrusters with applied magnetic field. In $3^{rd}$ *Russian-German Conference on Electric Propulsion Engines and their technical applications*, Stuttgart, Germany, June 1994.

[14]G.A. Dyuzhev, E.A. Startsev, S.M. Shkol'nik, and V.G. Yur'ev. Low-temperature erosionless cathode for high current densities. *Soviet Physics - Technical Physics*, 23(10):1207–1209, October 1978.

[15]D.B. Fradkin, A.W. Blackstock, D.J. Roehling, T.F. Stratton, M. Williams, and K.W. Liewer. Experiments using a 25 kW hollow cathode lithium vapor MPD arcjet. *AIAA Journal*, 8(5):886–894, May 1970.

[16]L.I. Ageyev, S.D. Grishin, V.G. Mikhalev, S.N. Ogorodnikov, and V.N. Stepanov. Characteristics of high-current plasma sources with a hollow cathode. *Radio Engineering and Electronic Physics-USSR*, 20(9):67–71, 1975.

[17]A. Brunet. Characteristics of interior positive-column of a hollow cathode discharge deduced from probe measurements. *C.R. Acad. Sc. Paris*, 21:813–816, May 1973. (In French).

[18]A. Brunet. Hollow-cathode arc - experimental study of plasma column inside cathode. *Revue de Physique Appliquee*, 12(8):1105–1110, August 1977. (In French).

[19]L.D. Cassady. *Lithium-fed Arc Multichannel and Single-channel Hollow Cathode: Experiment and Theory*. PhD thesis, Princeton University, September 2006.

[20]L.D. Cassady and E.Y. Choueiri. Experimental and theoretical studies of the lithium-fed multichannel and single-channel hollow cathode. In $29^{th}$ *International Electric Propulsion Conference*, Princeton University, NJ, USA, October-November 2005. IEPC-2005-094.

[21]J.D. Cobine. *Gaseous Conductors*. Dover, New York, 1958.

[22]G.V. Babkin and A.V. Potapov. An experimental investigaion of the effect of oxygen on the erosion of a multichannel tungsten cathode. *Journal Of Applied Mechanics And Technical Physics*, 3, 1979.

[23]W.G. Vincenti and Jr. C.H. Kruger. *Introduction to Physical Gas Dynamics*. Krieger Publishing Company, Malabar, FL, USA, 1965.

[24]C.M. Ferreira and J.L. Delcroix. Theory of the hollow cathode arc. *Journal of Applied Physics*, 49(4):2380–2395, April 1978.

[25]J. Lafferty. *Vacuum Science and Technology*. John Wiley & sons, New York, NY, USA, 1998.

[26]D. Santeler. Exit loss in viscous tube flow. *Journal of Vacuum Science and Technology A*, 4(3):348–352, 1986.

[27]D. Santeler. Gas-flow experiments in the transition region. *Journal of Vacuum Science and Technology A*, 12(4):1744–1749, July/August 1994.

[28]S. Chapman and T.G. Cowling. *The Mathematical Theory of Non-uniform Gases*. University Press, Cambridge, UK, 3rd edition, 1970.